Int. J. Electrochem. Sci., 13 **(2018)** 1527 – 1541, doi: 10.20964/2018.02.42

International Journal of
ELECTROCHEMICAL
SCIENCE
www.electrochemsci.org

Effect of Cooling Rate on Microstructure and Corrosion Behavior of Low Alloy Steel under H_2S/CO_2-saturated Saline Solution Environment

Chi Yu[1,2*], *Hongwei Wang* [3], *Xiuhua Gao* [4]

[1] School of Resources and Materials, Northeastern University at Qinhuangdao, Qinhuangdao 066004, China;
[2] School of Mechanical Engineering, Yanshan University, Qinhuangdao 066000, China;
[3] School of Control Engineering, Northeastern University at Qinhuangdao, Qinhuangdao 066004, China;
[4]The State Key Laboratory of Rolling and Automation, Northeastern University, Shenyang 110819, China
[*]E-mail: yuchi0319@163.com

Received: 21 August 2017 / *Accepted:* 24 October 2017 / *Published:* 28 December 2017

The effect of cooling rate on microstructure and corrosion behavior of low alloy steel exposed to H_2S and CO_2-saturated saline solution environment are investigated by means of immersion tests and electrochemical experiments. The microstructure, corrosion kinetics, surface morphology and cross-section morphology have been examined using optical microscope (OM), scanning electron microscope (SEM), energy-dispersive spectroscopy (EDS) and X-ray diffraction (XRD). The results show that the microstructure is refined with increasing cooling rate, the corrosion resistant performance is good. The corrosion products are $FeCO_3$, mackinawite, troilite and pyrrhotite, and mackinawite dominates the corrosion phases. It is seen that there is very compact corrosion products formed on the sample surface with immersion time, which will lead to decrease corrosion rate and effectively protect the steel substrate.

Keywords: low alloy steel; H_2S/CO_2; corrosion behavior; SEM; XRD

1. INTRODUCTION

In the oil and gas industry, the low alloy steel not only has good mechanical properties, but also has excellent corrosion resistance. The CO_2 corrosion (sweet corrosion) is an intractable problem in the process of oil and gas production and transportation, so some research works have been performed,

and the corrosion mechanism has been studied [1-4]. Additionally, H_2S gas generated through chemical and biological reactions is one of the toxic impurities in the oil and gas. When the water in oil and gas encounters H_2S and CO_2, and the corrosion behavior will become very complex. Apart from inducing sever general and localized corrosion, the presence of H_2S would cause hydrogen induced cracking (HIC) and sulfide stress corrosion cracking (SSCC) of pipelines and tubings [5-7]. The complex work conditions are easier to cause corrosion failure, which will bring serious accident and economic loss. So it is necessary to develop low alloy steel for oil and gas industry and study the comprehensive properties.

Recently, the corrosion problems about H_2S/CO_2 have attracted more attention because of their destruction behavior, and have obtained some results [8-14]. Masamura et al have proposed a critical ratio of P_{H_2S}/P_{CO_2} to understand the corrosion property of carbon steel, when $P_{H_2S}/P_{CO_2}<200$, the corrosion products are FeS and $FeCO_3$, when $P_{H_2S}/P_{CO_2}>200$, the corrosion products are mainly $FeCO_3$, and CO_2 plays an important role [15]. Pots et al have presented that when $P_{H_2S}/P_{CO_2}>500$, CO_2 plays an important role during corrosion process, when $P_{H_2S}/P_{CO_2}<20$, H_2S has a major influence on the whole reaction process, and when $20<P_{H_2S}/P_{CO_2}<500$, the corrosion behaviors are controlled by H_2S and CO_2 simultaneously[16]. Also some scholars have researched the corrosion properties of alloy steel in environment with high H_2S and CO_2 content and the results indicate that the H_2S has an important influence and precipitation of iron sulfide on the steel surface is superior to iron carbonate [8, 17-18]. Wei et al have investigated the effect of small amount of H_2S on the corrosion behavior of carbon steel in the CO_2 environment, and analyze the composition of corrosion products [19]. Zhao et al. have studied that the corrosion behavior about Ni-based alloys in simulation solution containing H_2S/CO_2 at different temperature [20]. Zhang et al have researched the effect of Cl^- accumulation on corrosion behavior of steel in H_2S/CO_2 solution [21]. Zhang et al. [22] study the corrosion behavior of carbon steel under dynamic high pressure H_2S and CO_2 environment, the results show the corrosion process switches to H_2S corrosion control with the increase of partial pressure ratio. They have investigated the effects of alloy elements Cr on corrosion resistance in CO_2/H_2S environment [23-24]. Ref [24] studies corrosion behavior of P110 grade tube steel under H_2S and CO_2 environment($P_{CO_2}/P_{H_2S}=15$) at 60°C, the total pressure is 0.1 MPa. Also between long immersion time and corrosion properties in H_2S and CO_2 environment are studied [25-26]. Yan et al [27] investigate the corrosion behavior of different types of materials. It is worth noting that most studies are performed for a certain kind of steel exposed to H_2S and CO_2 environment. Few studies have been reported in the literature concerning the corrosion behavior of low alloy steel by analysis rolling parameters and microstructure [28]. However, it is well known that the influences of microstructure on corrosion resistance of low alloy steel are very important. Therefore, to clarify its corrosion mechanism is essential.

In this paper, the corrosion properties of low alloy steel exposed to 3.5 wt% NaCl solution containing H_2S/CO_2 environment are studied to simulate the practical working environment of oil and gas industry, ($P_{CO_2}/P_{H_2S}=7$) at 75°C, the total pressure is 1.2 MPa by immersion experiment and electrochemical method. The mutual relationships of rolling parameters, microstructure and corrosion surface morphology are discussed. It can provide the basic theoretical reference to develop corrosion resistant steel for oil and gas industry.

2. EXPERIMENTAL PROCEDURE

The chemical composition of experiment steel is shown in Table 1. The steel is melted using a vacuum furnace, casted into ingots, forged into billet with dimension of 120 mm (high) × 100 mm (wide) × 110 mm (length). Then, the plate is rolled into 12 mm thickness at room temperature. The dynamic continuous cooling transformation (CCT) curve based on dilatometer and metallographic method is obtained by thermal simulation experiments, as shown in Fig.1. From the CCT curve, it is seen that the microstructure is mainly polygonal ferrite (PF) and little pearlite (P) when the cooling rate is low (< 2^{o}C/s). With the increase of cooling rate, the content of pearlite gradually decreases and the amount of bainite increases. When the cooling rate rises to more than 20^{o}C/s, the microstructure is acicular ferrite (AF) and martensite (M). It is known that the corrosion resistance with granular bainite and acicular ferrite steel is better and comprehensive mechanical properties are higher. So the cooling rate should be controlled the between 10^{o}C/s and 20^{o}C/s according to the results of CCT curve analysis.

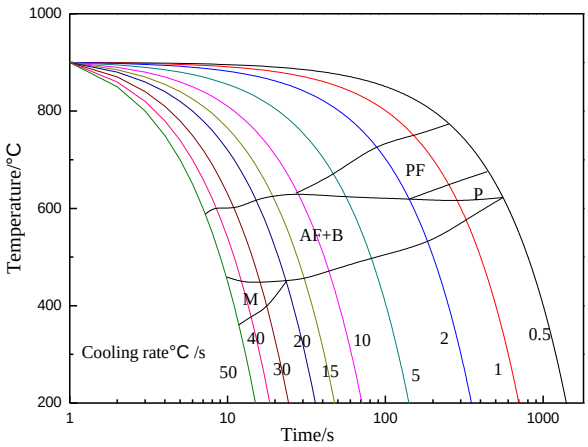

Figure 1. Dynamic CCT curves for the low alloy steel

Based on above analysis, the appropriate thermo mechanical control process (TMCP) rolling parameters are listed in Table 2. Three kinds of samples are obtained, which are marked as No.1, No.2 and No.3, respectively. The four parallel samples (three for mass loss measurement and one for rust layer analysis) are cut into the sizes of 20 mm × 25 mm × 4 mm. The electrochemical samples are cut into 10 mm × 10 mm × 3 mm, and only a surface with 10 mm×10 mm is exposed to the solution, other surfaces are isolated by epoxy resin. All samples are ground with a series of silicon carbide papers (100, 600, 800 and 1200), cleaned with distilled water and alcohol, then dried, weighted and stored in a moisture-free desiccator prior to use.

A high temperature and high pressure autoclave with 5 L volumn is the main reactor for immersion test and its schematic diagram is shown in Fig.2. The test electrolyte is 3.5 wt% NaCl (analytical grade reagent) solution. N_2 is bubbled into the electrolyte for 3 h to deoxygenate, and then H_2S/CO_2 are purged into for 1 h to saturate the solution at room pressure. After that, the electrolyte is heated to 75^{o}C and the total pressure is 1.2 MPa with partial pressure 0.09 MPa H_2S, 0.64 MPa CO_2

and 0.47 MPa N_2. Four immersion durations of 24 h, 48 h, 96 h and 192 h are chosen to study the corrosion mechanism. After immersion tests, three coupons for weight loss measurements are immediately cleaned with distilled water and alcohol respectively. The chemical method with the etching solution compositions of 50ml 37% HCl, 5g hexamethy lenetebramine (urotropine) and 450ml deionized water is chosen to descale the scale, the role of hexamethy lenetebramine is to inhibit effectively the chemical dissolution of steel substrate. The corrosion rate (v) is calculated according to the following equation

$$v = \frac{8.76 \times 10^4 \times \Delta m}{S \times t \times \rho} \quad (1)$$

where v is the average corrosion rate, mm/year, Δm is the mass loss, g; S is the total exposed surface area, cm^2; t is the immersion duration, h; ρ is the density of low alloy steel.

The electrochemical experiments are performed with PATSTAT2273 workstation. A conventional three-electrode cell is used for the polarization curve test. A platinum electrode is used as the auxiliary electrode, a saturated calomel electrode (SCE) is used as the reference electrode, and the low alloy steel is used as the working electrode. All polarization curves are obtained with scan rate of 0.1 mV/s. The mixed gas is continuously poured in the aerated 3.5 wt% NaCl solution with partial pressure 0.09 MPa H_2S, 0.64 MPa CO_2 and 0.47 MPa N_2, the electrolyte is kept at 75 ^oC.

Table 1. Chemical composition of low alloy steel (wt %)

C	Si	Mn	P	S	Al	Cr	Cu	W	Mo	Ni	Nb	Fe
0.085	0.24	1.36	0.006	0.002	0.04	0.23	0.16	0.21	0.21	0.11	0.012	balance

Table 2. TMCP rolling process parameters

Samples	Start finish rolling temperature / ^oC	Final rolling temperature / ^oC	Final cooling temperature / ^oC	Cooling rate / $^oC \cdot s^{-1}$
No. 1	859	851	665	9.9
No. 2	856	856	642	12.7
No. 3	851	853	614	15.9

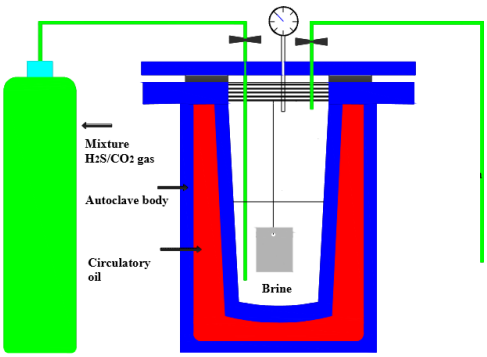

Figure 2. Schematic diagram of autoclave setup

The microstructures are observed by using LEICA optical microscope (OM) and FEI QUANTA 600 scanning electron microscopy (SEM). The electron back scattered diffraction (EBSD) are performed on FEI/Philips quanta 600 to investigate crystallographic characteristics maps and grain size. The surface morphology of corrosion products is examined by ZEISS ULTRA55 field emission scanning electron microscope equipped with EDS. Corrosion phases are detected using X-ray diffraction (XRD) with Co Kα radiation and a step of 0.02^{o} and identified by matching peak positions automatically with MDI Jade software.

3. RESULTS AND DISCUSSION

3.1 Microstructure

The microstructure characteristics of experiment steels No.1, No.2 and No.3 are shown in Fig.3.

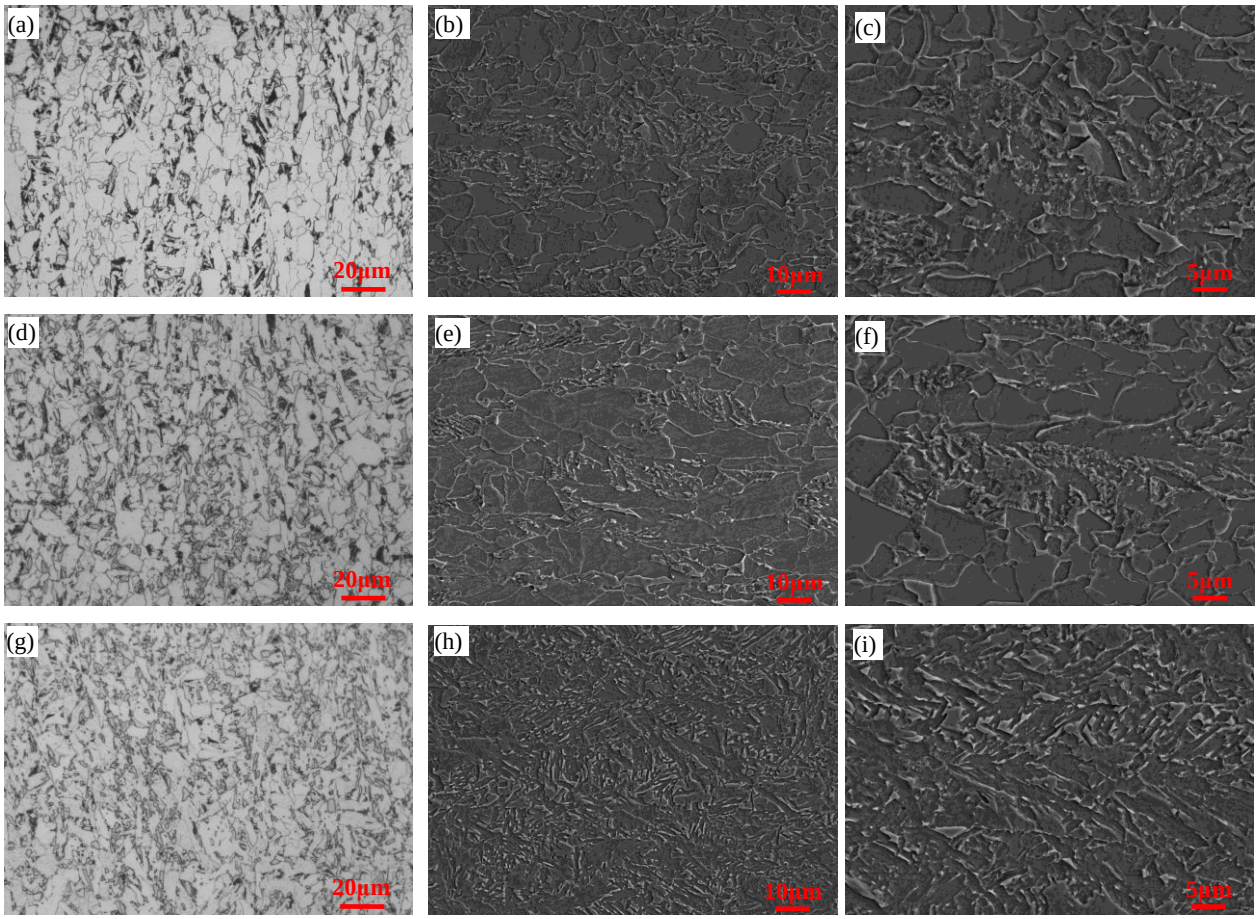

Figure 3. The OM and SEM images for the experimental steels No.1 (a, b, c), No.2 (d, e, f) and No.3 (g, h, i)

The type of microstructures is quasi polygonal ferrite, granular bainitic and lath bainitic. They are very similar to each other, polygon ferrite grain size is large, and the distribution is relatively

concentrated for No.1 steel. However, the ferrite grain of No.2 and No.3 is relatively small, the grains are refined, and the distribution of bainite is more uniform. The more lath bainite are observed in No.3 steel, which can be attributed to its faster cooling rate.

Fig.4 shows that the area fraction of different grain size. It is seen that the area fraction of fine grain for No.3 steel will much more than steels No.1 and No.2. Under the same rolling temperature condition, with decrease final cooling temperature, ferrite grains are refined, granular bainite morphology are becoming more obvious, the lath bainite have been found in No.3 steel. The reason may be that the transformation of granular bainite is a process of nucleation and growth, and the temperature affects the growth rate of grain. The low final cooling temperature can increase the nucleation rate of bainite, but difficult to promote granular bainite crystal nucleus to grow up, instead, the high final cooling temperature can accelerate the grow up of granular bainite, result in appearing the coarse granular bainite.

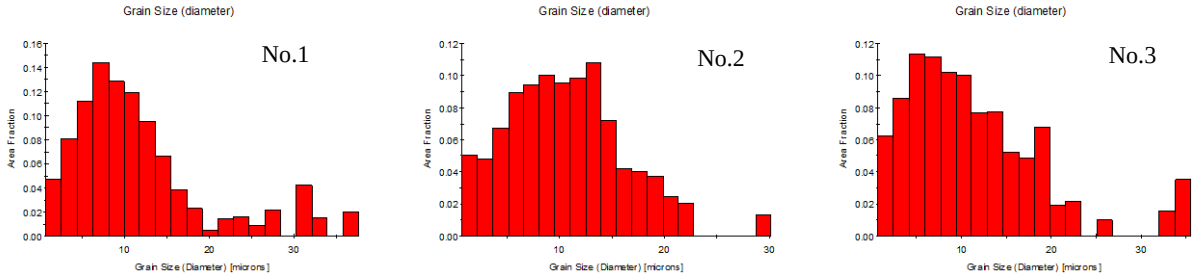

Figure 4. The area fraction of experimental steel vs. grain size

3.2 Corrosion Kinetics

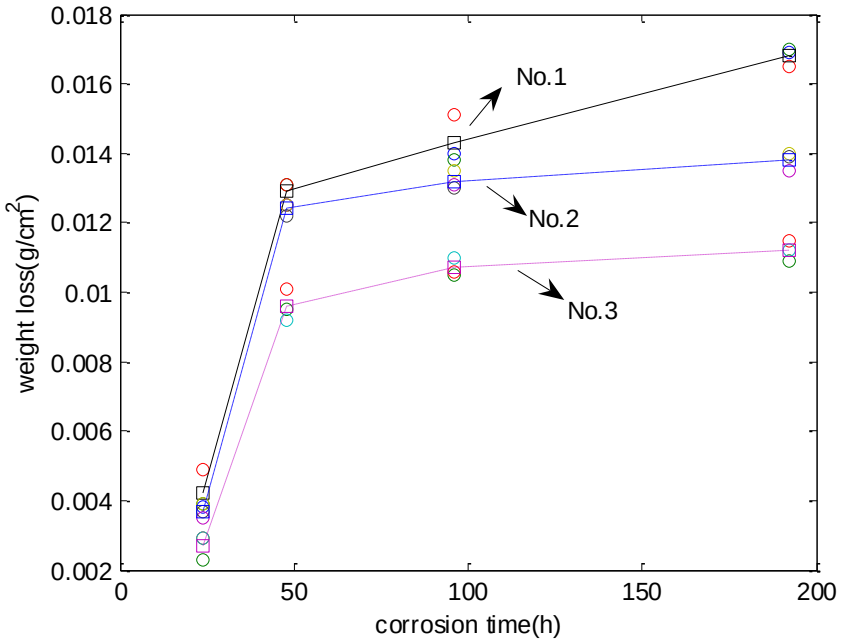

○: scatter value, □: average value

Figure 5. The mass loss curve of experiment steel

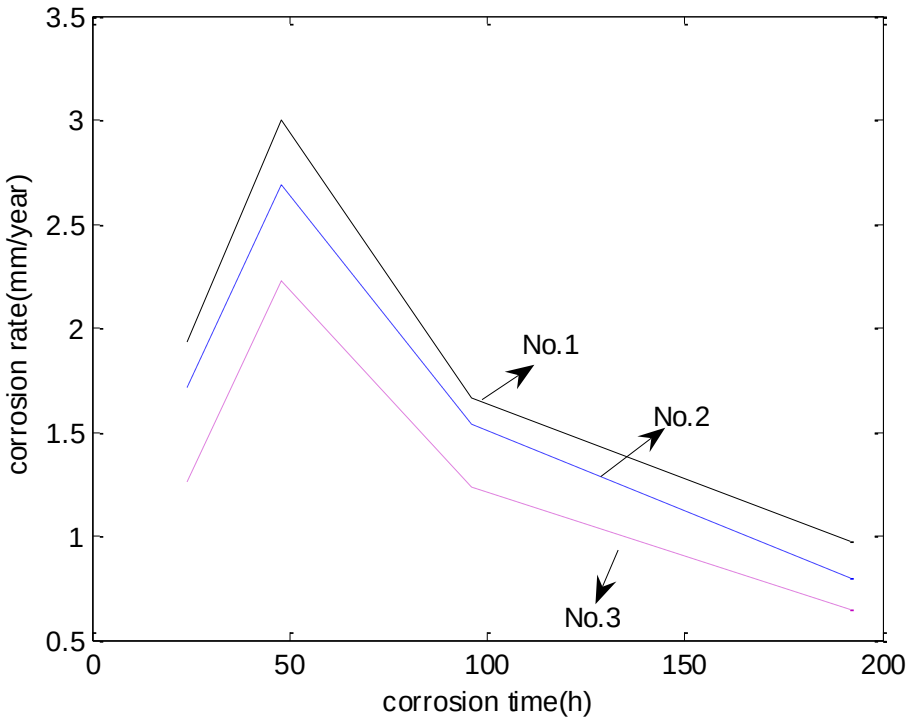

Figure 6. The corrosion rate curve of experiment steel

The mass loss and average corrosion rate of experiment steel are shown in Fig.5 and Fig.6, respectively. They reveal the corrosion property of materials.

It is found that the mass loss is also varied with immersion time. It exhibits three distinguishable stages. At the first stage (0 h to 48 h), the mass loss increases sharply. At second stage from 48 h to 96 h, the weight loss increment is low. At the end of this stage (96 h to 192 h), weight loss slowly increases, and reaches a platform. Fig.6 demonstrates the corrosion rate increases firstly and then decreases. The transition points in the corrosion process are 48 h. The transition point could depend on when the compact corrosion product layer appears, which will be interpreted further. The corrosion rate of No.3 steel is lower than other steels, it indicates that the corrosion resistance depends on the steel microstructure and grain size, which may be result from the different cooling rate.

3.3 Corrosion Phases

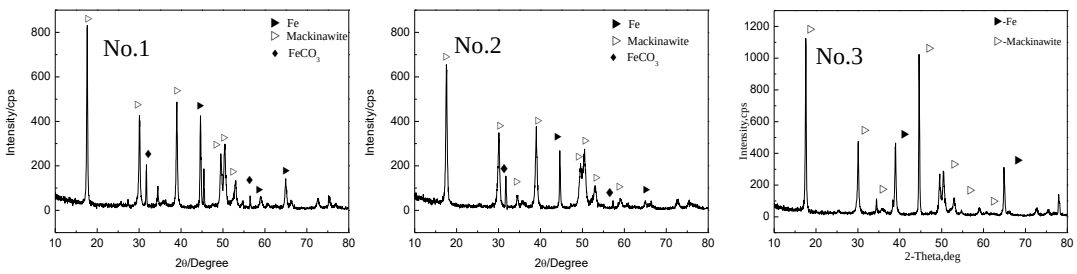

Figure 7. XRD of experimental steel in H_2S and CO_2 environment at 75^oC after immersion 48h

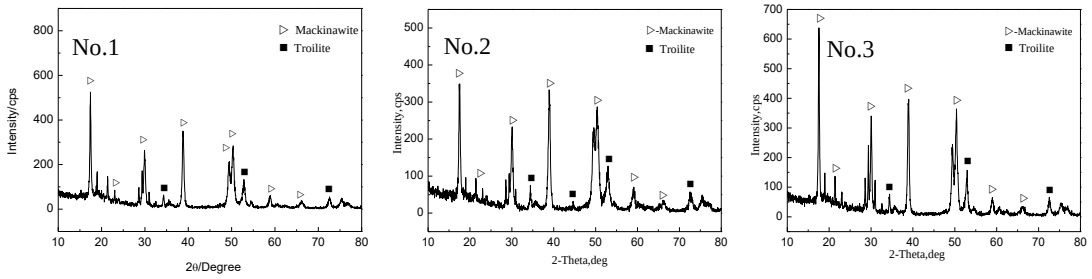

Figure 8. XRD of experimental steel in H_2S and CO_2 environment at 75^oC after immersion 96h

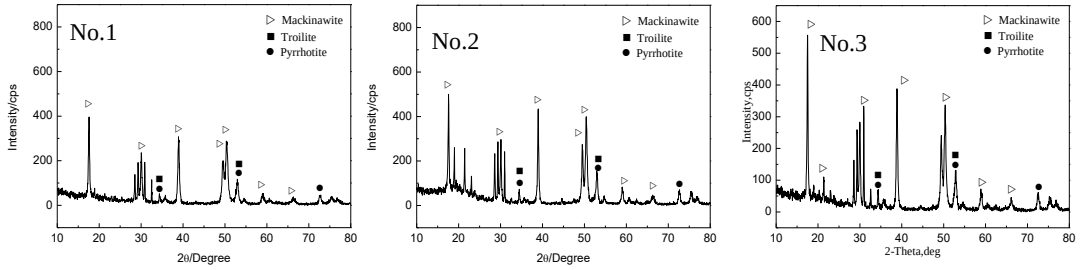

Figure 9. XRD of experimental steel in H_2S and CO_2 environment at 75^oC after immersion 192h

Fig.7-Fig.9 list the results of XRD pattern. It shows that the main corrosion phase is diversity of H_2S corrosion product, $FeCO_3$ and Fe are detected in the early stage. The majority of strong peak come from mackinawite is occurred in the spectra. When immersion time is 48h, the pattern of $FeCO_3$ is not observed for No.3 steel. Only Fe is remained when the test steel immersed for 48h. This result can be attributed to the thin corrosion films formed during earlier immersion times because only a few corrosion products exist at this time. Approximately 96h later, the steel surface is covered with only diversity of H_2S corrosion product. It indicates that the H_2S corrosion has a significant effect on the whole reaction process and iron sulfide is superior to precipitating on the steel surface compared with iron carbonate.

3.4 Surface morphology

Fig.10 shows the surface morphology of experiment steel in sodium chloride solution containing H_2S and CO_2. The corrosion behavior of steel is influenced by the structural properties of corrosion product. The dense and compact corrosion products are beneficial to improve the corrosion resistance [29, 30]. So the structural properties of corrosion product are studied. It is seen that the corrosion mechanism of experimental steel is essentially the same from the Fig.10. Based on the previous studies[31, 32], it is found that the layer of corrosion products has formed on the steel surface of 24h and 48h immersion, these tetragonal corrosion crystals are mackinawite, the corrosion particle is large and loose, and the steel substrate is not fully covered by corrosion products, the local position generates corrosion crack, the gaps are possible to be passages that the corrosion solution diffuses into the inner layer and even into the substrate surface, the phenomenon has a bad influence on the

corrosion resistance. As the corrosion scales mainly composed of mackinawite grow thicker, it will crack and fall off as a result of stress due to the volume effect, therefore the corrosion product is very loose [26-28]. With the increase of soaking time, mackinawite is formed and dissolved, and the nucleation and growth of troilite and pyrrhotite occupy a certain position, the corrosion products will change from mackinawite to troilite and pyrrhotite [33]. Obviously, the corrosion scales after immersion 192 h are very compact, the protective ability of corrosion product films increases and corrosion rate decreases. In general, the regular and dense scale can impede the corrosive ions through the scale, which is a well protection for the steel matrix. The absence of iron carbonate in the corrosion scales indicates that the corrosion process is main governed by H_2S control. As immersion time increases, the particles of steel No.3 are much more uniformity and denser than those of steels No.1 and No.2, and a flake-like tetragonal crystals mackinawite are formed on the coupon surface in the corrosion later period, the corrosion resistant performance is good, which can be attributed to its microstructure.

In the H_2S/CO_2 corrosion environment, the reaction is mainly CO_2 corrosion when the partial pressure of H_2S is small, the reaction is mainly H_2S corrosion when the partial pressure of H_2S is high [8, 34]. In our experiments, the partial pressure of H_2S is high, iron sulfide crystals are the main corrosion products. The electrochemical reactions of experiment steel are very complicated in H_2S/CO_2 environment. There are various species in the solution, such as H^+, CO_3^{2-}, HCO_3^-, HS^-, S^{2-} and Fe^{2+} ions [35]. The cathode reaction are shown as follows.

$$2H^+ + 2e \rightarrow H_2$$

$$2H_2CO_3 + 2e \rightarrow 2HCO_3^- + H_2$$

$$2HCO_3^- + 2e \rightarrow 2CO_3^{2-} + H_2$$

$$H_2S \rightarrow HS^- + H^+$$

$$2HS^- + 2e \rightarrow 2S^{2-} + H_2$$

The anodic reaction is mainly the dissolution of steel and the formation of corrosion product, which are shown as follws.

$$Fe \rightarrow Fe^{2+} + 2e$$

$$Fe + H_2CO_3 \rightarrow FeCO_3 + H^+ + 2e$$

$$Fe + H_2S \rightarrow FeS_{1-x} + xHS^- + (2-x)H^+ + 2e$$

During the process of corrosion, the irreversible chemical reaction between Fe and H_2S is fast, although the concentration of H_2S in water is relatively small [31]. The formation of corrosion products comprise a series of electrochemical reactions. The mackinawite are the initial corrosion products , then transformed into other iron sulfide, such as troilite and pyrrhotite.

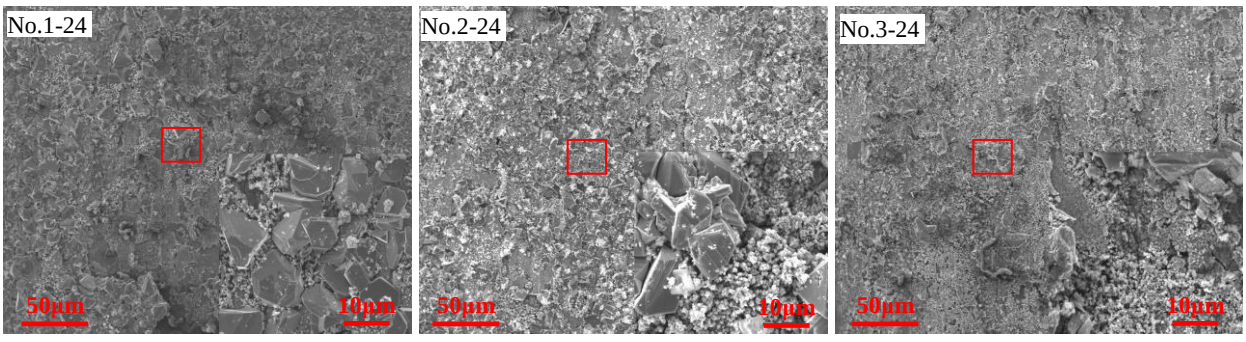

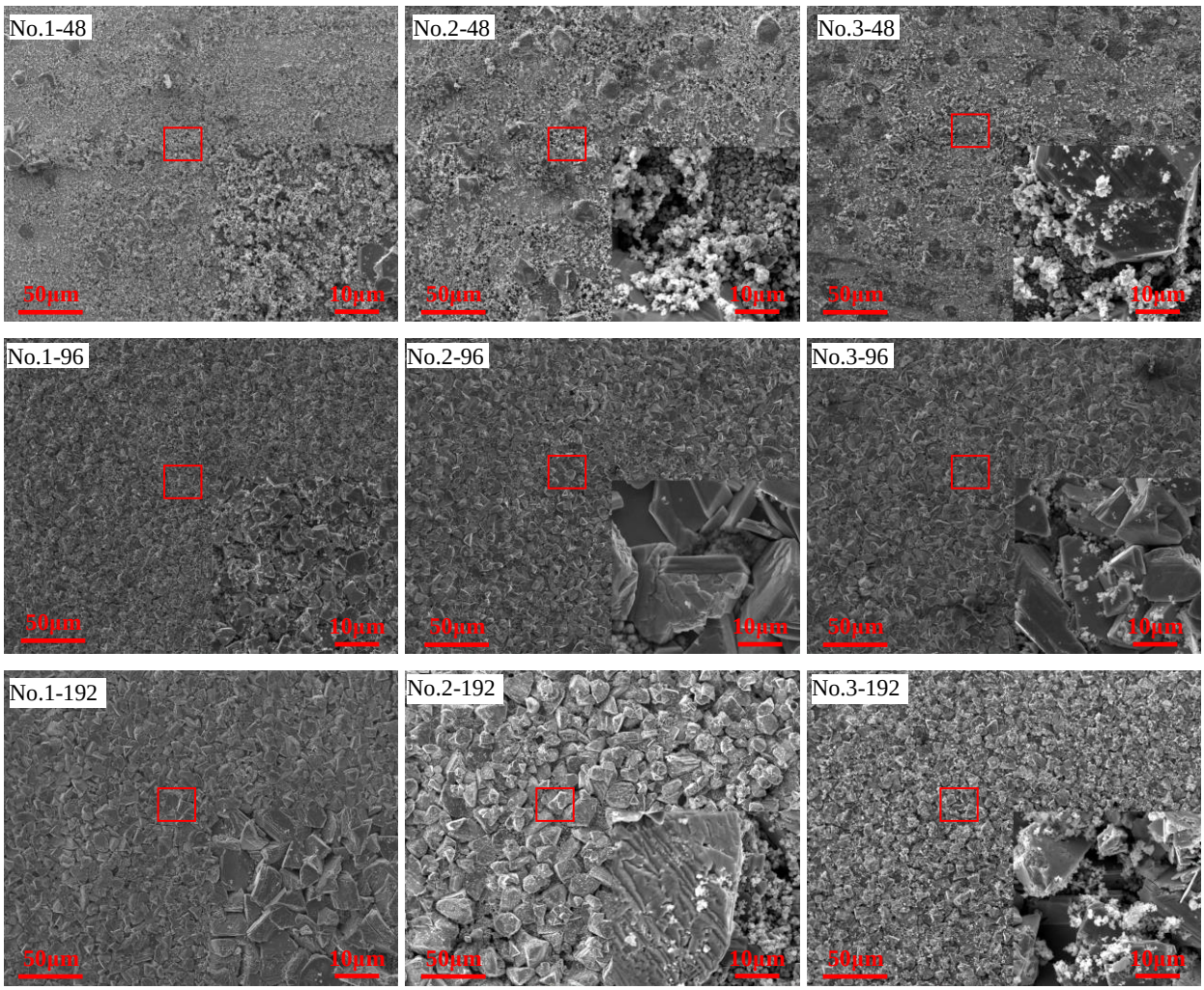

Figure 10. SEM images of corroded surface for experimental steels No.1, No.2 and No.3 in H_2S and CO_2 environment at 75°C after different immersion durations

3.5 Cross section morphology

Fig.11 shows cross section morphology characterization and reveals the thickness of corrosion rust. After 24 h immersion, a loose inner layer about 5 μm-10 μm and a porous outer layer ranging from 0 μm to 8 μm are formed on the coupon surface. After immersion 48 h, the inner layer is damaged, a discontinuous inner layer is attached on the steel substrate. With immersion time goes by from 96 h to 192 h, the thickness of the inner layer grow. The inner layer of the coupons is more compact. That acts as a shield to resist eroding further. Outer layer of the coupons of 192 h immersion duration is thicker than one of 96 h immersion duration, it is more uniform with thickness about 30 μm. And inner layer and outer layer of No. 3 steel are better than one of steels No.1 and No.2 in each corrosion cycle. The corrosion product is distributed homogeneously on the coupon surface. It demonstrates No. 3 steel has good corrosion resistance, consistence with the surface morphology results. The pitting sites are not found from the cross-sectional morphology. Thus, the experimental

steel is free of pitting corrosion and suitable for use of tubing steel, and it has excellent corrosion resistance to pitting corrosion.

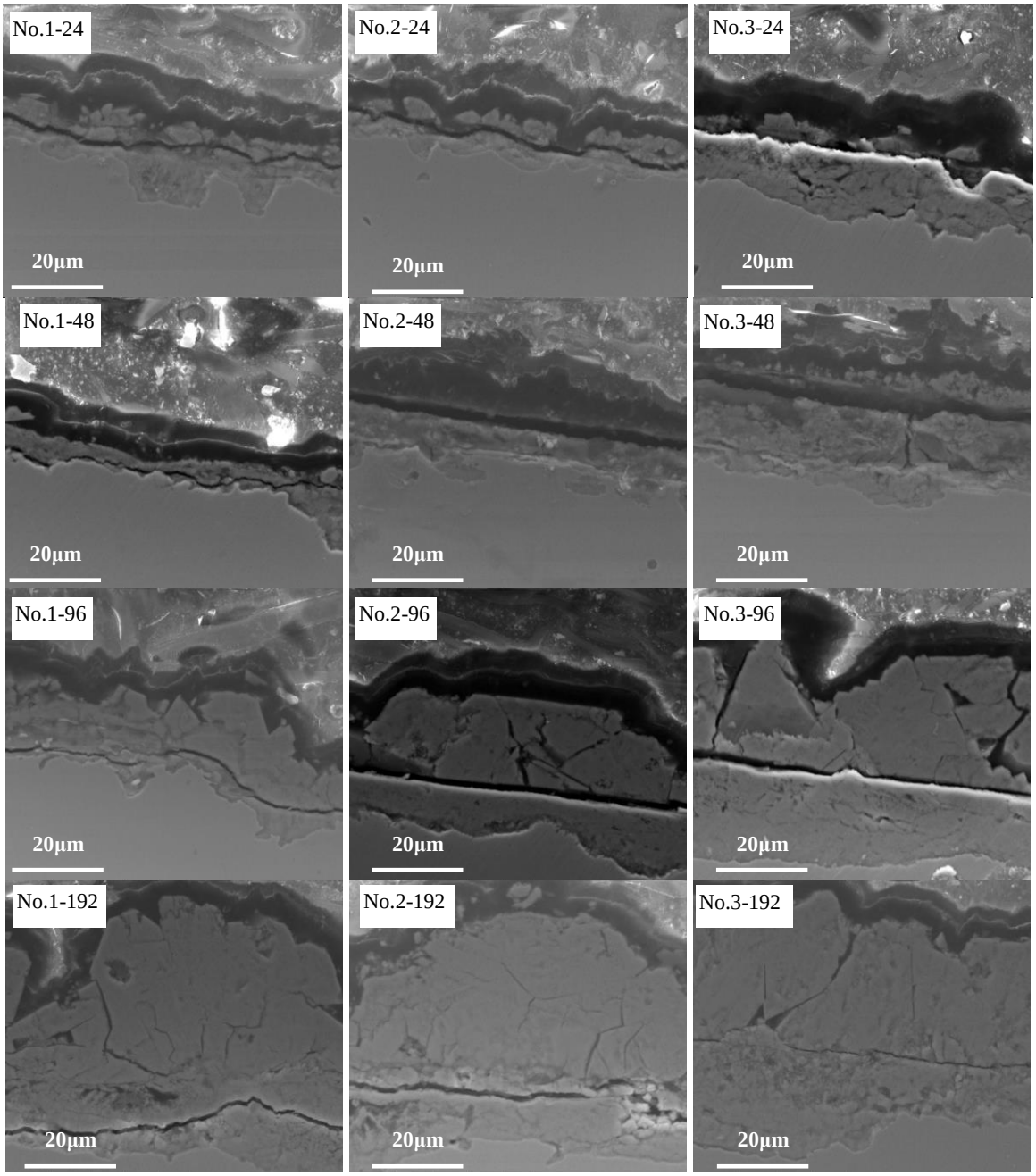

Figure 11. Cross-section morphology of experimental steel in H_2S and CO_2 environment at 75°C different immersion durations

3.6 Potentiodynamic polarization curve measurement

Fig.12 gives the potentiodynamic polarization curves of experimental steels after different immersion time. The corresponding fitting parameters such as anodic tafel constants (b_a), cathodic tafel constants (b_c), corrosion potential (E_{corr}) and corrosion current density (I_{corr}) are shown in Table 3.

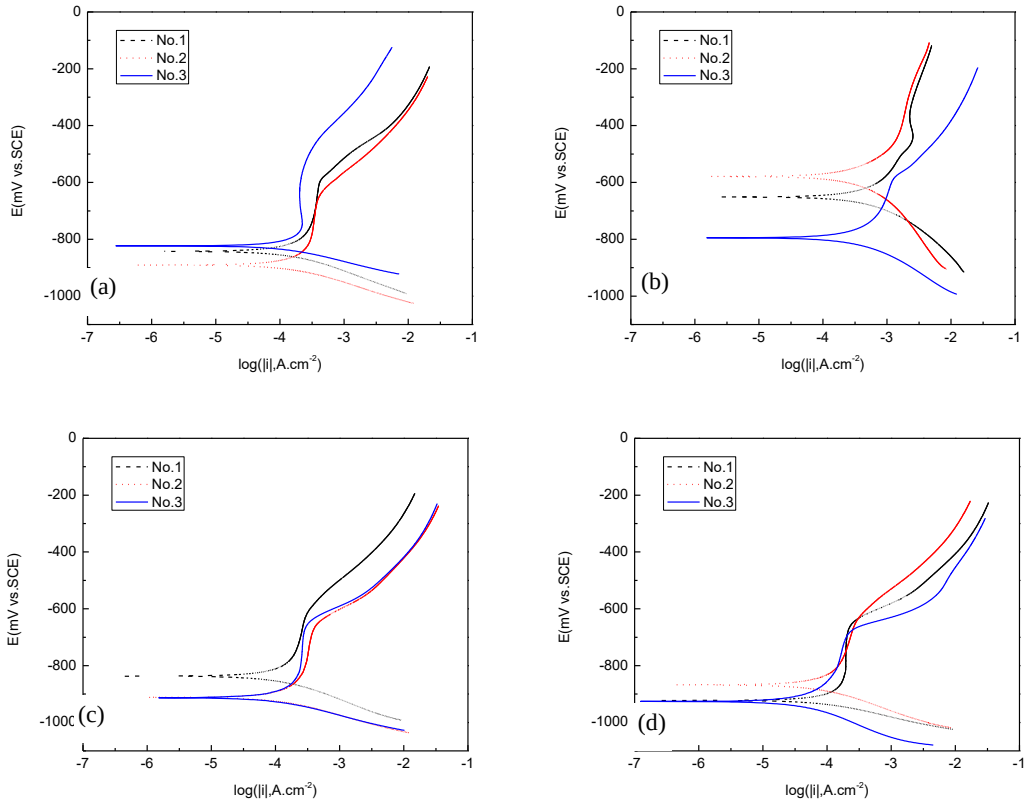

Figure 12. Potentiodynamic polarization curves of steels No.1, No.2 and No.3 in H_2S and CO_2 environment at 75°C after different immersion (a)24 h (b)48 h(c)96h and (d)192h

The corrosion current density decreases simultaneously with immersion time increase from 48 h to 192 h, it will show denser corrosion product films are formed on Fe surface for 192 h. The corrosion rate v is calculated by substituting corrosion current density taken from Tafel plot for the following equation [36].

$$v = 0.00327 \frac{ai}{nD} \qquad (1)$$

where a is molar mass of steel (g/mol), i is corrosion current density ($\mu A/cm^2$), n is valency, D is steel density. It is seen that the high corrosion current density represents big corrosion rate, it will be more prone to corrosion [37-38].

Fig.13 gives the curve of corrosion current density. It is found that the largest corrosion rate is observed at 48 h based on the equation (1), the varying tendencies of potentiodynamic polarization curves are all consistent with accelerated corrosion tests, the corrosion data are correct. Our previous experiments show the similar results, showing that the corrosion data correct [28]. The corrosion current of No.3 experimental steel is 0.07 when the immersion time reaches to 192 h, and the corresponding corrosion rate is small. It show the good corrosion resistance, which is mainly due to reasonable rolling parameters.

Table 3. Potentiodynamic polarization parameters from a curve-fitting approach

Immersion time/hour	Sample	b_a(mV/dec)	b_c(mV/dec)	E_{corr}(mV vs.SCE)	I_{corr}(mA.cm^{-2})
24	No.1	923	-98	-842	0.26
	No.2	927	-84	-891	0.25
	No.3	529	-72	-823	0.23
48	No.1	797	-213	-651	1.21
	No.2	447	-350	-579	0.91
	No.3	1157	-186	-795	0.87
96	No.1	1024	-100	-837	0.19
	No.2	481	-73	-912	0.17
	No.3	552	-69	-913	0.16
192	No.1	882	-62	-923	0.14
	No.2	487	-91	-868	0.12
	No.3	329	-108	-926	0.07

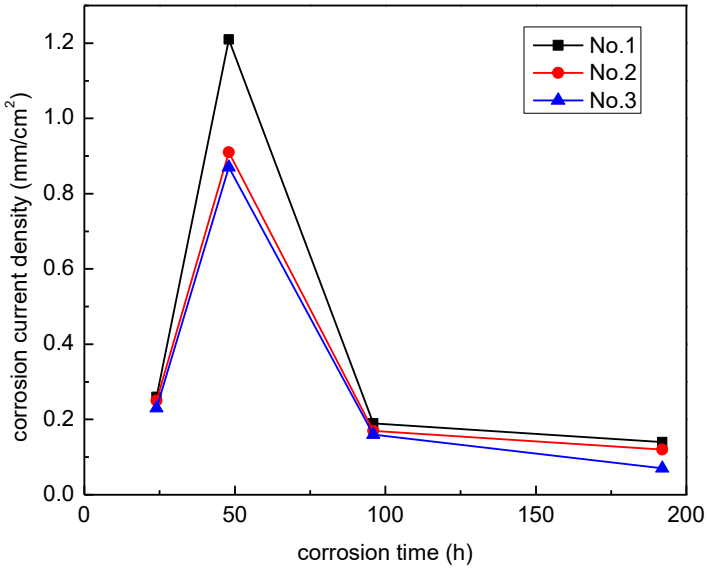

Figure 13. The corrosion current density curve of experiment steel

4. CONCLUSIONS

The effect cooling rate on corrosion behavior of low alloy steel is studied in H_2S/CO_2 -saturated saline solution environment. The corrosion properties are investigated by the microstructure, corrosion kinetics, corrosion phases, surface morphology and cross-section morphology. According to the test results, the microstructure of experimental steel is quasi polygonal ferrite and bainitic, the grain is refined with cooling rate increases. The corrosion process is governed by H_2S control. The corrosion products are mainly composed of different types of iron sulfide. The transformation process of corrosion products involves the following sequence: mackinawite/ troilite →mackinawite/ troilite/ pyrrhotite. The mackinawite crystals control the corrosion process, and troilite and pyrrhotite crystals are minor corrosion product. The corrosion rate of steel No.3 is lower than No.1 and No.2 by

immersion test and electrochemical method under the whole corrosion process, which can be attributed to its faster cooling rate. With increase immersion time, the variation of corrosion products and compactness of corrosion layer will decrease the corrosion rate to improve the corrosion resistance.

ACKNOWLEDGEMENT
This work was supported by the Scientific Research Fund Project of Northeastern University at Qinhuangdao (No.XNB201717), the Technology Support Project of Northeastern University at Qinhuangdao (No.XNK201604), the Science and Technology Project of Hebei Province (No.15211028), and the Nature Science Foundation of Liaoning Province (No. 20170540310)

References

1. G. A. Zhang and Y. F. Cheng, *Electrochim. Acta*, 56(2011)1676.
2. Z. G. Liu, X. H. Gao, C. Yu, L. X. Du, J. P. Li and P. J. Hao, *Acta Metall. Sin*., 28 (2015) 739.
3. F. F. Eliyan and A. Alfantazi, *Corros. Sci*., 85(2014)380.
4. L. Q. Chen, J. Zhou, Y. X. Chen, P. P. Bai, J. Wu and S. Q. Zheng, *Int. J. Electrochem. Sci*., 11(2016) 3987.
5. M. A. Lucio-Garcia, J. G. Gonzalez-Rodriguez, M. Casales, L. Martinez, J. G. Chacon-Nava, M. A. Neri-Flores and A. Martinez-Villafane, *Corros. Sci*., 51(2009)2380.
6. M. Al-Mansour, A. M. Alfantazi and M. Ei-boujdaini, *Mater. Design*, 30(2009)4088.
7. E. Ramírez, J. G. González-Rodriguez, A. Torres-Islas, S. Serna, B. Campillo, G. Dominguez-Patiño and J. A. Juárez-Islas, *Corros. Sci*., *50*(2008)3534.
8. W. F. Li, Y. J. Zhou and Y. Xue, *J. Iron Steel Res. Int*., 19(2012)59.
9. W. He, O. Ø. Knudsen and S. Diplas, *Corros. Sci*., 51(2009)2811.
10. L. D. Paolinelli, T. Pérez and S. N. Simison, *Corros. Sci*., 50(2008)2456.
11. X. H. Hao, J. H. Dong, J. Wei, W. Ke, C. G. Wang, X. L. Xu and Q. B. Ye, *Acta Metall. Sin*., 48(2012)534.
12. Z. Aslam, R. A. Shawabkeh, I. A. Hussein, A. Al-baghli and M. Eic, *Appl. Surf. Sci*., 327(2015)107.
13. H. S. Song, M. G. Park, E. Croiset, Z. W. Chen, S. C. Nam, H. J. Ryu and K. B. Yi, *Appl. Surf. Sci*., 280(2013) 360.
14. S. Upasen, P. Batocchi, F. Mauvy, A. Slodczyk and P. Colomban, *J. Alloy Compd*., 622(2015)1074.
15. K. Masamura and S. Hashizume, *Corros*., 43(1987)359.
16. B. F. M. Pot, S. D. Kapusta and R. C. John, *In: corrosion 2002, Houston, 2002*.
17. P. Y. Wang, J. Wang, S. Q. Zheng, Y. M. Qi, M. X. Xiong and Y. J. Zheng, *Int. J. Hydrogen Energ*., 40(2015) 11925.
18. C. Plennevaux, J. kittel, M. Frégonèse, B. Normand, F. Ropital, F. Grosjean and T. Cassagne, *Electrochem. Commun*., 26(2013)17.
19. L. Wei, X. L. Pang and K. W. Gao, *Corros. Sci.*, 103(2016)132.
20. X. H. Zhao, Y. Han, Z. Q. Bai and B. Wei, *Electrochim. Acta*, 56(2011) 7725.
21. N. Y. Zhang, D. Z. Zeng, G. Q. Xiao, J. F. Shang, Y. Z. Liu, D. C. Long, Q. Y. He and A. Singh, *J. Nat. Sci. Eng*., 30(2016) 444.
22. G. A. Zhang, Y. Zeng and X. P. Guo, *Corros. Sci.*, 65(2012)37.
23. L. D. Wang, H. B. Wu, Y. T. Liu, H. W. Zhang, L. F. Liu and D. Tang, *Mater. Sci. Technol*., 21(2013)8.
24. H. B. Wu, L. F. Liu, L. D. Wang and Y. T. Liu, *J. Iron Steel Res. Int*., 21(2014)76.
25. C. Yu, P. Wang and X. H. Gao, *Int. J. Electrochem. Sci*., 10(2015) 6820.
26. H. W. Wang, P. Zhou, S. W. Huang and C. Yu, *Int. J. Electrochem. Sci*., 11(2016)1293.

27. W. Yan, P. K. Zhu and J. G. Deng, *Int. J. Electrochem. Sci*., 11(2016)9542.
28. H. W. Wang and C. Yu, *Int. J. Electrochem. Sci*., 12(2017)4327.
29. D. P. Li, L. Zhang, J. W. Yang, M. X. Lu, J. H. Ding and M. L. Liu, *Int. J. Min. Metall. Mater.*, 21(2014)388.
30. Z. F. Yin, L. Liu, Y. Q. Zhang, K. Wang and S. D. Zhu, *Corros. Eng. Sci. Technol*., 47(2012)138.
31. P. P. Bai, H. Zhao, S. Q. Zheng and C. F. Chen, *Corros. Sci*., 93(2015)109.
32. F. X. Shi, L. Zhang, J. W. Yang, M. X. Lu, J. H. Ding and H. Li, *Corros. Sci*., 102(2016)103.
33. Y. L. L, R. A. Van and S. T. Weber, *J. Solid State Chem.*, 181(2008)3151.
34. C. Q. Ren, D. X. Liu, Z. Q. Bai and T. H. Li, *Mater. Chem. Phys*., 93(2005)305.
35. L. Wei, X. L. Pang and K. W. Gao, Corros. Sci. 103(2016)132-144.
36. M. Liu, J. Q. Wang, W. Ke and E. H. Han, *J. Mater. Sci. Technol*., 30(2014) 504.
37. M. N. Ilman, *Eng. Fail. Anal*., 2(2014)1.
38. S. W. Kim and H. W. Lee, *Int. J. Electrochem. Sci*., 9(2014)4709.